ADVANCED FUNCTIONAL MATERIALS
www.afm-journal.de

# Superhydrophobic, Surfactant-doped, Conducting Polymers for Electrochemically Reversible Adsorption of Organic Contaminants

*Yinying Ren, Zhou Lin, Xianwen Mao, Wenda Tian, Troy Van Voorhis, and T. Alan Hatton**

**Polymeric adsorbents show great potential for the replacement of activated carbon for removing a wide range of toxic organic pollutants from wastewater streams since they do not suffer from costly regeneration needs and high attrition rates. Herein, an electrochemically regenerable polymeric adsorbent based on an intrinsically conducting polymer (CP), polypyrrole (PPy), doped with anionic surfactant dioctylsulfosuccinate (AOT), denoted PPy(AOT), for mitigating organic pollutants in wastewater is reported. A facile electropolymerization protocol to synthesize highly porous PPy(AOT) is developed, with an adsorption capacity of greater than 570 mg pollutant/g polymer in its superhydrophobic oxidized state. It is demonstrated that the hydrophobicity of PPy(AOT) and hence its affinity for organics can be modulated electrochemically through the re-orientation of AOT dopants, which can be exploited to regenerate the adsorbent and use it repeatedly for multiple adsorption/desorption cycles. It also explores the interactions between the adsorbed organic molecules and the surfactant-doped CP adsorbent using a combined density functional theory and molecular dynamics approach to elucidate the mechanism of electrochemical modulations of hydrophobicity and affinity of the material. The physicochemical insights are significant for developing broader applications of such material in drug delivery, sensing, self-cleaning surfaces, microfluidics, and artificial muscles.**

## 1. Introduction

The presence of organic contaminants such as synthetic chemicals, pesticides, and pharmaceuticals and personal care products in industrial, agricultural, and municipal wastewaters is an emerging and pressing issue.[1,2] The lack of efficient methods to remove organic contaminants, especially uncharged species in the micromolar range, further hinders remediation of their negative effects on aquatic ecosystems and human health.[3–5] Adsorption is a common technology for removing organic pollutants from wastewater, and activated carbon (AC) is one of the most widespread adsorbents due to its high specific surface area and strong interactions with target compounds.[6–8] Methods for AC regeneration have drawbacks, however, thermal desorption is energy-intensive, while solvent regeneration may lead to substantial loss of AC and result in secondary pollution.[7–10] To overcome recyclability problems such as observed with AC, our group has previously developed a redox-responsive polymer gel with tunable hydrophobicity that reversibly adsorbs and releases organics in the presence of water.[11] However, in this case, the redox switching relied on the addition of chemicals, which introduced additional chemical agents to the remediation process, and the efficacy of the chemical stimuli was hampered by mass transfer limitations.[11,12] Therefore, it is desirable to design new adsorbent materials whose redox-responsive hydrophobicity can be tuned using mild electrical stimuli, thereby eliminating the use of chemicals in the regeneration process, and ultimately reducing the material waste and operating cost of adsorption technology for wastewater remediation. We have addressed this problem by developing two different methods for electrochemical control of the hydrophobic environment within the adsorbent, by ferrocene redox-responsive moieties similar to those described above,[13] and the approach adopted in this paper.

Herein, we present proof of concept of electrochemically reversible adsorption for the removal of neutral organic pollutants from water. This technology relies on a reusable adsorbent material based on a conducting polymer (CP) doped with anionic surfactants whose affinity for organic molecules can be modulated by electrochemical redox stimuli. We synthesized the CP on a conductive carbon fiber cloth substrate and simultaneously doped the polymer with surfactants using a one-step electropolymerization process. The as-synthesized CP possessed a highly porous morphology and was superhydrophobic in its oxidized state as evidenced by a water contact angle of 152.1° ± 1.8°. The morphological and compositional advantages of the CP also enabled the material to manifest redox

Y. Ren, Dr. X. Mao, Dr. W. Tian, Prof. T. A. Hatton
Department of Chemical Engineering
Massachusetts Institute of Technology
77 Massachusetts Avenue, Cambridge, MA 02139, USA
E-mail: tahatton@mit.edu
Dr. Z. Lin, Prof. T. Van Voorhis
Department of Chemistry
Massachusetts Institute of Technology
77 Massachusetts Avenue, Cambridge, MA 02139, USA
The ORCID identification number(s) for the author(s) of this article can be found under https://doi.org/10.1002/adfm.201801466.

**DOI: 10.1002/adfm.201801466**

state-dependent hydrophobicity and hence disparate affinities for neutral organic micropollutants. We explored the mechanism of hydrophobicity and affinity modulations by simulating the surfactant–CP–adsorbate interactions using a combination of density functional theory (DFT) and molecular dynamics (MD). Finally, we demonstrated that the surfactant-doped CP can be used as a regenerable adsorbent for removing neutral organic contaminants from water. The regeneration relies on the ability to control the hydrophobicity and the affinity of the adsorbent electrochemically: a simple electrochemical reduction step renders the CP hydrophilic, releasing the previously adsorbed pollutant molecules to a small volume of stripping solution (water), and thereafter making the polymer available for another cycle of adsorption.

## 2. Results and Discussion

### 2.1. Electrochemical Modulation of Hydrophobicity

#### *2.1.1. Synthesis of Surfactant-Doped Polypyrrole*

The electrochemical reversibility of an adsorption process requires adsorbent materials that are electrically conducting and exhibit tunable affinity for target contaminants in response to electrochemical stimuli. Polypyrrole (PPy) is a promising candidate for enabling electrochemical regeneration due to its intrinsic conductivity, fast electrochemical switching, low operating voltage, and relative ease of fabrication and potential modulation of its hydrophobicity through doping of the polymer with anionic surfactants.[14,15] A typical oxidative polymerization reaction of pyrrole yields CP in the oxidized state, and hence anions are incorporated into the polymer backbone during synthesis to neutralize the positive charges of the oxidized polymer. The size of the anionic dopants dictates whether the doping and dedoping are associated mainly with cations or anions during subsequent redox reactions of PPy.[16] Small anions can be easily inserted into PPy when it is oxidized and de-inserted when the polymer is reduced, as depicted in **Figure 1**a. However, bulky surfactant anions doped into PPy during synthesis are largely immobile. Therefore, subsequent reduction of the CP is accompanied by insertion of cations from the electrolyte to neutralize the charges of those immobilized surfactant anions (Figure 1b).[17]

The choice of anionic dopants also affects the hydrophobicity of the resulting PPy. For example, a PPy film doped with perfluorooctanesulfonate (PFOS) or dodecylbenzenesulfonate (DBS) exhibited hydrophobicity while perchlorate-doped PPy was hydrophilic.[15,18] Moreover, on electrochemical switching of the redox state of PPy doped with perfluoro or alkyl sulfonate surfactants, the polymer exhibited changes in hydrophobicity: the oxidized PPy was more hydrophobic than the reduced polymer.[15,18] However, the loss of PFOS during electrochemical reduction of PPy required the use of fluorochemicals during subsequent reoxidation of PPy to replenish the dopants,[18,19] which may have resulted in even worse contamination than caused by the original contaminants.[20] Unlike PFOS, surfactants with long alkyl chains such as DBS are believed to be retained during redox switching, and the re-orientation of the surfactant anions with respect to the PPy results in a hydrophobic/hydrophilic transition.[15,21] Therefore, in this work, we chose to dope PPy with alkyl sulfonates and relied on their bulky hydrophobic tails to modulate the hydrophobicity of PPy. We proposed to take advantage of the one additional alkyl chain in dioctylsulfosuccinate (AOT) to induce larger hydrophobicity swings than possible with DBS-doped PPy. The polypyrroles prepared in this work are identified according to the nomenclature PPy("dopant"). For example, PPy(AOT) refers to polypyrrole doped with AOT.

We synthesized the surfactant-doped CP by electropolymerizing pyrrole dissolved in an AOT aqueous electrolyte in the presence of a trace amount of bipyrrole (pyrrole dimer, 0.75 mol%). The resulting PPy(AOT) film was deposited on a flexible commercial carbon fiber cloth substrate and had hierarchical porosity, as observed in the scanning electron microscopy (SEM) images (Figure 1c); this porous polymer is denoted as P-PPy(AOT). In contrast, we carried out the electropolymerization in the absence of bipyrrole and obtained a compact non-porous film, denoted as NP-PPy(AOT) (Figure 1d). The surface roughness factor derived from the 3D atomic force microscopy (AFM) images (Figure 1d,e), defined as the ratio of the actual surface area and the projected surface area,[22] was 1.92 and 1.07 for P-PPy(AOT) and NP-PPy(AOT), respectively. A nearly doubling in surface roughness in P-PPy(AOT) further supports the observation of porosity enhancement in the CP electropolymerized in the presence of bipyrrole. Despite the difference in morphology, the chemical compositions of P- and NP-PPy(AOT) were identical as evident by the Fourier-transform infrared spectroscopy and X-ray photoelectron spectroscopy (XPS) spectra (Figure S2a,b, Supporting Information). The sulfur (S) peaks in XPS spectra also confirmed the presence of AOT dopants within the CP in both cases.

#### *2.1.2. Electrochemical Modulation of Hydrophobicity*

To examine the electrochemical modulations of the hydrophobicity of the surfactant-doped polymer, we measured the contact angle of a water droplet on the surfaces of various PPy samples coated on stainless-steel substrates (Figure S4a, Supporting Information). The greater the contact angle is, the more hydrophobic is the surface. Larger water contact angles were measured on all three types of oxidized PPy films, namely P-PPy(AOT), NP-PPy(AOT) and P-PPy(DBS), compared with their respective reduced films (**Table 1**).

Furthermore, it has been established in the literature that both composition effects and geometrical structure influence the hydrophobicity of a surface.[23] That is, both the type of dopant and the porosity of the film affected the hydrophobicity of PPy. Although similar morphological and electrochemical behavior was observed in the NP- and P- PPy(DBS) (Figure S3, Supporting Information), P-PPy(AOT) was more hydrophobic than P-PPy(DBS) in both the oxidized and reduced states (Table 1). This observation validates our hypothesis that AOT dopants can increase the hydrophobicity of the polymer over that of DBS owing to its additional alkyl chain. More importantly, a larger difference in contact angles between oxidized and reduced states was observed in P-PPy(AOT) than in P-PPy(DBS) (108° versus 95°), suggesting AOT is the better

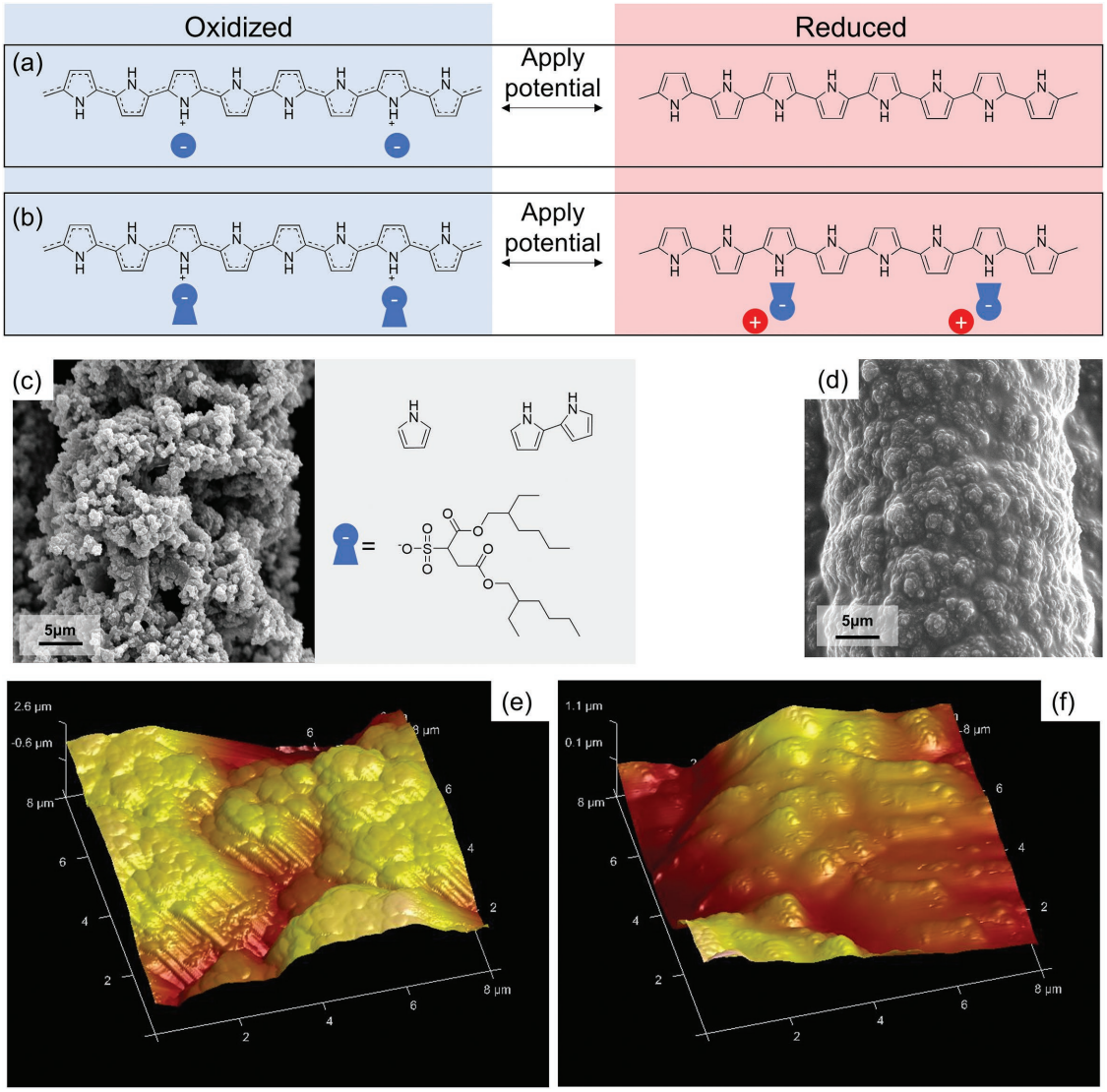


**Figure 1.** Schematic illustrations for two different ion exchange processes during the oxidation and reduction of PPy doped with (a) small anions and (b) bulky surfactant anions. c) An SEM image of porous AOT-doped PPy film electropolymerized and deposited on a carbon fiber cloths substrate in the presence a trace amount of bipyrrole (0.75 mol%), denoted as P-PPy(AOT), and structures of pyrrole monomer, bipyrrole, and an AOT surfactant. d) An SEM image of compact AOT-doped PPy film electropolymerized without bipyrrole, denoted as NP-PPy(AOT). 3D AFM images showing height variations on the surface of part (e) P-PPy(AOT) and part (f) NP-PPy(AOT) films.

dopant compared to DBS, as it increases the window for hydrophobicity switching.

On the other hand, surface roughness can induce the so-called "lotus effect" and its impact on water contact angles can be characterized by the Wenzel model[22]

**Table 1.** Contact angle measurements of a water droplet on the surface of stainless-steel substrates coated with PPy films in oxidized or reduced states doped with AOT or DBS anions.

| Polymer film | Oxidized | Reduced | Difference |
|---|---|---|---|
| P-PPy(AOT) | 152.1° ± 1.8° | 43.8° ± 3.1° | 108.3° |
| NP-PPy(AOT) | 55.6° ± 4.2° | 13.3° ± 1.9° | 42.3° |
| P-PPy(DBS) | 117.1° ± 2.5° | 22.5° ± 2.2° | 94.6° |

$$\cos\alpha = r\cos\alpha_0 \quad (1)$$

where $\alpha_0$ is the water contact angle on an ideal, smooth, and homogeneous PPy(AOT) surface and $r$ is the surface roughness factor measured using AFM. The rougher surface of P-PPy(AOT) renders its oxidized state superhydrophobic (152.1° ± 1.8°),[24,25] as well as amplifies the difference between its oxidized and reduced states in comparison with that of NP-PPy(AOT) (108° versus 42°).[26]

Contact angle measurements suggest that P-PPy(AOT) is the most promising candidate for an electrochemically regenerable adsorbent, with a superhydrophobic oxidized state for adsorption and a larger hydrophobicity disparity to lower the affinity for organics in the reduced state and thereby drive desorption.

#### 2.1.3. Electrochemically Modulated Affinity for Organics

We investigated whether the ability to electrochemically modulate the hydrophobicity of surfactant-doped PPy can be translated into affecting the affinity of the polymer towards organic pollutant molecules. Herein, we selected three model compounds, namely Sudan Orange G (SOG), a neutral organic molecule representing an important class of organic pollutant–azo dye molecules widely used in textile, paper, food, cosmetics, and pharmaceutical industries; propranolol hydrochloride (PP), a beta-blocking pharmaceutical agent; and bisphenol A (BPA), a component of plastics and epoxy resins and also an endocrine disruptor. **Figure 2**a,c,e compare the equilibrium distribution coefficient (L $g^{-1}$ polymer) defined as

$$K_d = Q_e / C_e \quad (2)$$

which is the ratio of the amount of the pollutant adsorbed per gram of polymer ($Q_e$) to the concentration of the pollutant in the solution phase ($C_e$), for SOG and PP at an initial concentration of $0.01 \times 10^{-3}$ M, and BPA at $0.02 \times 10^{-3}$ M, in contact with the oxidized and reduced NP-PPy(AOT) and P-PPy(AOT) coated on carbon fiber cloths. The oxidized NP- and P-PPy(AOT) both demonstrated a greater $K_d$ than the respective reduced polymers, indicating that the oxidation of PPy(AOT) activated the polymer to exhibit higher affinity for the neutral organic pollutants. In particular, the difference in $K_d$ between the oxidized and reduced states was even more dramatic for P-PPy(AOT), in agreement with the earlier observation of a greater disparity in contact angle measurements in the more porous film. The highly porous morphology also increased the surface area of PPy(AOT) for adsorbing organic molecules. For example, the equilibrium SOG distribution coefficient for the oxidized P-PPy(AOT) ($K_d$ = 44.1) was 3.3 times as high as oxidized NP-PPy(AOT) ($K_d$ = 13.3).

The adsorption thermodynamic properties of the better-performing P-PPy(AOT) are presented in Figure 2b,d, f. In the low concentration regime, the experimental data can be fitted with linear isotherms, indicating operation in the Henry's Law regime. The larger slope of the curve for the oxidized P-PPy(AOT) (the Henry's Law constant) further confirmed its stronger affinity for the organic pollutants. We also tested the capacity of the P-PPy(AOT) for adsorbing SOG from water over a wide range of concentrations (Figure 2b inset), which can be fitted well with the Freundlich adsorption isotherm

$$Q_e = k C_e^{1/n} \quad (3)$$

The Freundlich exponent $1/n$ is related to favorableness of adsorption—the degree of favorableness increases as $1/n$ approaches zero.[27] For oxidized and reduced P-PPy(AOT), the fitted $1/n$ values were 1.5 and 1.8, respectively, consistent with the fact that the oxidized polymer has a higher affinity for SOG. Moreover, the equilibrium solid phase concentration reached a maximum of 578 mg SOG per gram polymer when the initial liquid phase concentration was at the solubility limit. The fitting parameters for both Freundlich and Henry's Law isotherms can be found in Table S1 (Supporting Information) for SOG, as well as in Table S2 (Supporting Information) for PP and Table S3 (Supporting Information) for BPA.

### 2.2. Investigations of Molecular Interactions

#### 2.2.1. Physicochemical Interactions in the PPy(AOT) Complex

The ability to modulate the hydrophobicity and the affinity for organics electrochemically in surfactant-doped CP, as reflected by changes in the water contact angles and adsorption affinity after application of redox stimuli, has been attributed to a re-orientation of the surfactant molecules.[15,21] In the oxidized state of PPy, AOT or DBS anions with negatively charged sulfonate groups are bound to the positively charged PPy backbone via electrostatic attractions, leaving the alkyl chains pointing away from the polymer backbone. The hydrophobic alkyl chains constitute the surface layer of the polymer film, causing a relatively large water contact angle. In the reduced state, on the other hand, the PPy backbone becomes less positively charged, if not completely neutral. The absence of the electrostatic attractions between AOT and PPy allows AOT molecules to rotate freely and re-arrange themselves such that more sulfonate groups and fewer alkyl chains are exposed at the outermost surface, rendering the surface hydrophilic and decreasing the water contact angle. During the reduction process, sodium ions might also enter the PPy film to neutralize the charges of the immobilized anions.

To validate the aforementioned hypothesis about surfactant re-orientation upon oxidation/reduction of the PPy backbone, we calculated the surfactant–PPy interactions in the oxidized and reduced states using a combination of DFT and MD. The DFT-optimized geometries of the PPy(AOT) complexes in the gas phase (**Figure 3**a,b) provided initial configurations for the MD simulations in the aqueous environment. In agreement with the aforementioned assertion, the MD trajectory of the oxidized PPy(AOT) complex shows that the sulfonate groups constituting the hydrophilic heads of the AOT anions exhibit strong electrostatic attractions with the oxidized and positively charged PPy backbone and orient themselves towards PPy (Figure 3c, and Movie S1, Supporting Information). In contrast, upon an artificial "reduction" of PPy, the hydrophilic heads of the AOT anions tend to re-orient away from the neutral PPy backbone due to the decreased strength of attractions and eventually constitute the surface layer of the PPy film (Figure 3d, and Movie S2, Supporting Information). Our calculations also show that the minimum distance between a sulfur atom in the hydrophilic heads of AOT and a carbon atom in the polymer backbone increases from 6.01 ± 0.64 to 6.75 ± 0.43 Å upon reduction, rendering a quantitative description of the reorientation (Figure 3e).

The total binding energy $E_{bind}$ of the oxidized PPy(AOT) complex (69.8 ± 5.7 kcal $mol^{-1}$ in the aqueous environment and 82.4 ± 3.4 kcal $mol^{-1}$ in the gas phase) is approximately seven to eight times that of the reduced PPy(AOT) complex (9.8 ± 2.5 kcal $mol^{-1}$ in the aqueous environment and 10.3 ± 1.6 kcal $mol^{-1}$ in the gas phase), corroborating the observed shorter distance between AOT and PPy when it is oxidized (Figure 3f). The total binding energies calculated

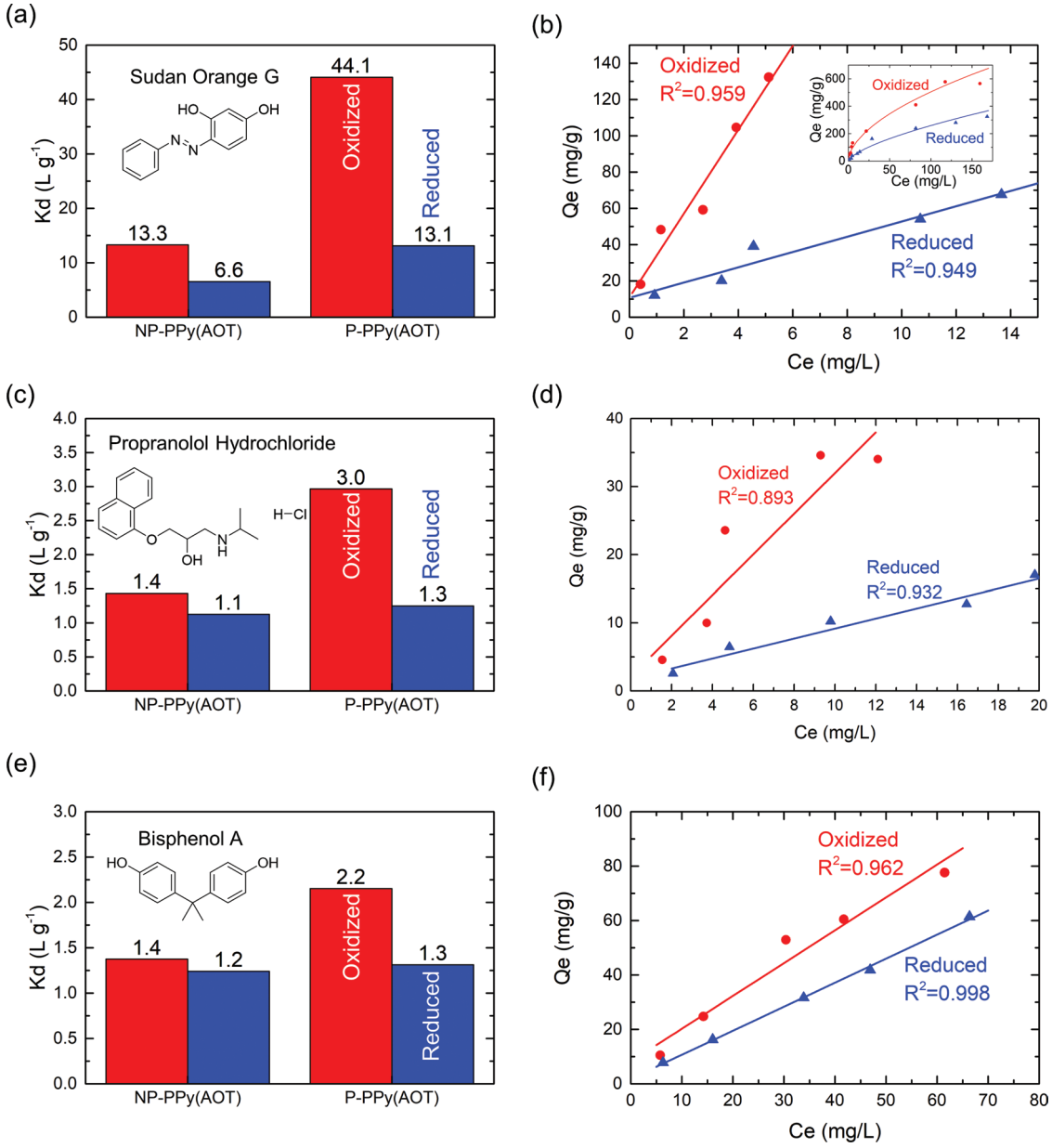


**Figure 2.** Equilibrium distribution coefficient $K_d$ of part (a) SOG with an initial concentration ($C_{ini}$) of $0.01 \times 10^{-3}$ M, c) PP ($C_{ini} = 0.01 \times 10^{-3}$ M), and e) BPA ($C_{ini} = 0.02 \times 10^{-3}$ M) on NP- and P-PPy(AOT) in oxidized and reduced states. The chemical structures of the organic compounds are provided in the insets. Adsorption isotherms of parts (b) SOG, (d) PP, and (f) BPA in oxidized and reduced states fitted with the linear model in the low concentration regime. b, inset) Equilibrium adsorption for a wide range of SOG concentrations fitted with the Freundlich isotherm. Line: fitted isotherms; symbols: experimental data; red: oxidized; and blue: reduced.

in the gas phase agree well with those obtained from the aqueous environment, and the slight overestimation in the gas phase can be ascribed to the partial screening of electrostatic and polarization interactions between AOT and PPy by water molecules. We further quantified the difference of the non-covalent interactions between AOT and PPy in oxidized and reduced states, and deconvoluted the relevant contributions of the intermolecular interactions using energy decomposition analysis (EDA) based on absolutely localized molecular orbitals (ALMO-EDA).[28–30] The gas-phase ALMO-EDA shows that the electrostatic attraction $E_{elec}$ contributes to the majority of the enhanced interactions between AOT and oxidized PPy—the value of $E_{elec}$ of the oxidized PPy(AOT) is almost seven times higher than that of the reduced PPy(AOT) (**Table 2**, 66.7 ± 4.4 versus 9.9 ± 3.3 kcal mol$^{-1}$). The charge-transfer stabilization $E_{CT}$ in oxidized PPy(AOT) is an order of magnitude higher than its reduced counterpart (9.8 ± 2.5 versus 0.8 ± 0.4 kcal mol$^{-1}$), although the charge-transfer contribution is smaller than can be attributed to electrostatics. Other non-bonding interactions include Pauli repulsion $E_{Pauli}$,[31] dispersion stabilization $E_{disp}$, and polarization stabilization $E_{pol}$, which remain almost unaffected in the redox process. In addition, although

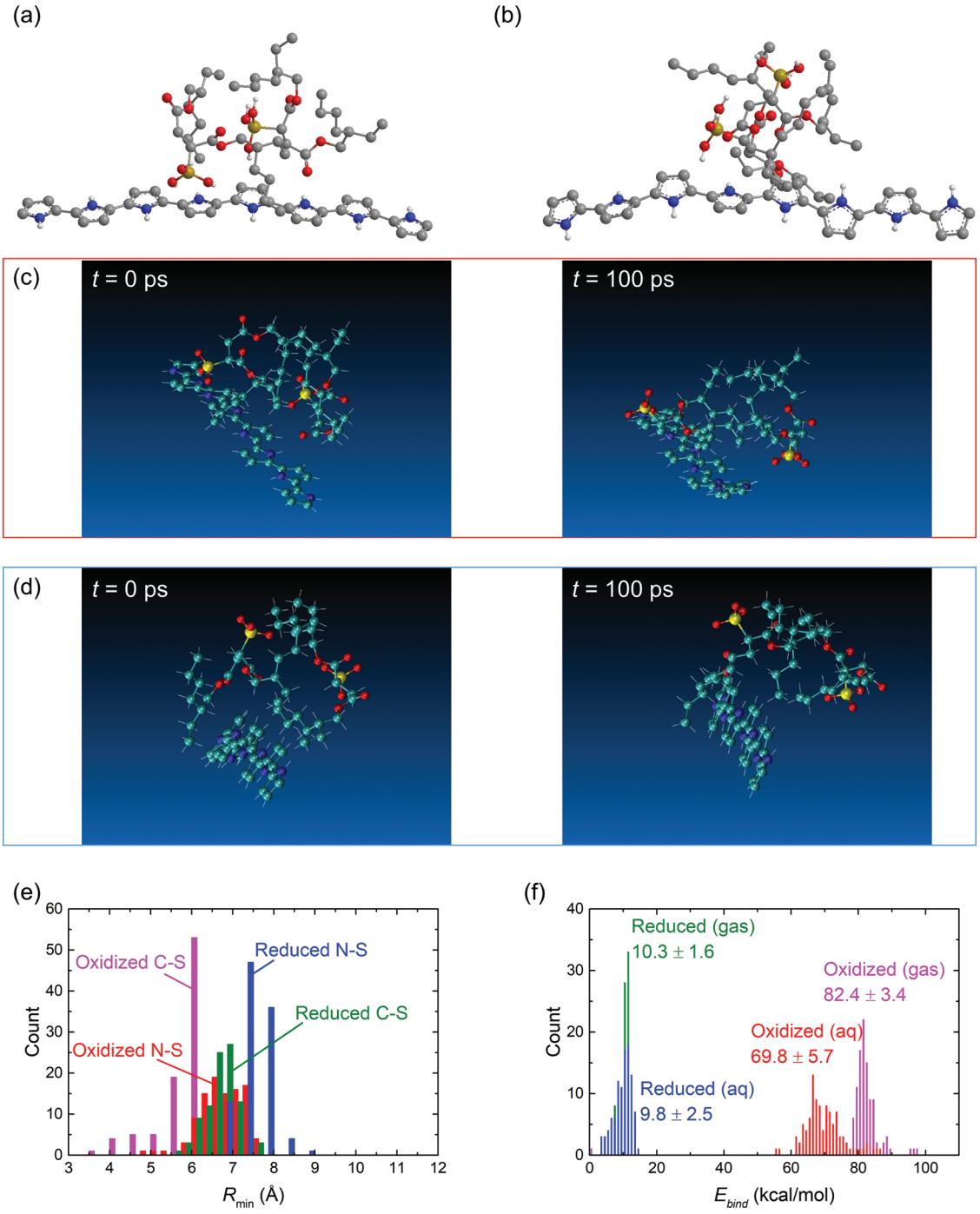


**Figure 3.** DFT-optimized geometries of PPy(AOT) complexes in the parts (a) oxidized and (b) reduced states showing the distinct orientations of AOT dopants relative to the PPy backbone. The atomic color schemes include gray (carbon), blue (nitrogen), yellow (sulfur), red (oxygen), and white (only polar hydrogen atoms are shown). Snapshots of MD simulations of parts (c) oxidized and (d) reduced PPy(AOT) complexes in aqueous solutions at $t = 0$ and 100 ps. All hydrogen atoms are shown as white sticks. e) Statistical results of minimum distance (Å) between one of the sulfur atoms in AOT and one of the carbon or nitrogen atoms in PPy, indicating that the distance between the dopant and the polymer is smaller when PPy is oxidized. f) Statistical results of total binding energy (kcal mol$^{-1}$) between AOT and PPy in the gas phase and the aqueous solution in oxidized and reduced states, showing stronger binding of AOT to PPy when it is oxidized, regardless of the media considered.

the reduced PPy(AOT) complex exhibits a weaker interaction, its intermolecular binding energy in the aqueous environment (9.8 ± 2.5 kcal mol$^{-1}$) is still twice as much as a typical hydrogen bond in water (≈4 to 5 kcal mol$^{-1}$),[32] and is much higher than that between chloride anions and reduced PPy (2.1 ± 0.6 kcal mol$^{-1}$), and hence is strong enough to prevent AOT from straying away from PPy at room temperature. Our DFT calculations and MD simulations provided theoretical and

**Table 2.** Statistical results of binding energies and their EDA between PPy and an AOT anion (in kcal mol$^{-1}$) in the gas phase.

| State | Binding $E_{bind}$ | Electrostatic $E_{elec}$ | Pauli repulsion $E_{Pauli}$ | Dispersion $E_{disp}$ | Polarization $E_{pol}$ | Charge transfer $E_{CT}$ |
|---|---|---|---|---|---|---|
| Oxidized | 82.4 ± 3.4 | 66.7 ± 4.4 | −10.2 ± 3.0 | 11.9 ± 1.7 | 4.3 ± 1.4 | 9.8 ± 2.5 |
| Reduced | 10.3 ± 1.6 | 9.9 ± 3.3 | −13.5 ± 4.4 | 10.5 ± 1.6 | 2.6 ± 0.6 | 0.8 ± 0.4 |

quantitative evidence for surfactant reorientation during redox reactions of PPy, which in turn leads to the changes in hydrophobicity of the polymer observed on the macroscopic scale.

#### 2.2.2. Adsorbent–Adsorbate Interactions

The configurational study of oxidized and reduced PPy(AOT) complexes reveals the geometric rearrangement in the complex in response to electrochemical redox stimuli. This behavior warrants further exploration of the molecular interactions between the PPy(AOT) complex in different oxidation states and the adsorbate molecule. DFT calculations in the gas phase are sufficient for providing representative molecular configurations and quantitative assessment of the adsorbate–adsorbent interaction energies.[33] The optimized geometry of an isolated SOG molecule (**Figure 4**a) is planar owing to the delocalized $\pi$-conjugation across two aromatic rings connected via the aryl azo structure. The introduction of the reduced PPy(AOT) complex allows the SOG to orient itself in parallel with the conjugated PPy backbone due to a $\pi$–$\pi$ stacking interaction (Figure 4b, and Movie S3, Supporting Information). In addition to the $\pi$–$\pi$ interaction, SOG also forms a moderate to strong hydrogen bond with the oxidized PPy(AOT), indicated by the short distance (2.65 Å) between the hydrogen atom in one of the hydroxyl groups of SOG and one of the oxygen atoms the in the sulfonate group of AOT (Figure 4c, and Movie S4, Supporting Information). An auxiliary ALMO-EDA study shows that the binding energies between SOG and PPy(AOT) in the reduced and oxidized states are 19.5 and 31.8 kcal mol$^{-1}$, respectively. The enhanced adsorbate–adsorbent interactions when PPy(AOT) is oxidized is due to a combination of strong electrostatic, polarization and charge-transfer interactions, while the dispersion stabilization is dominant when PPy(AOT) is reduced. Intuitively, the small distance and the hydrogen bonds foster a higher affinity of SOG to the oxidized PPy(AOT) in which the sulfonate groups of AOT orient towards the PPy backbone to allow stronger adsorbate–adsorbent interactions. The mechanistic understanding of the interaction of the PPy(AOT) complex with SOG suggests the electrochemical redox process of PPy(AOT) can mediate the separations of uncharged aromatic contaminant species containing hydrogen bond donors. Hydrogen bond donors are present in many neutral organic contaminants, including the two aforementioned species propranolol hydrochloride and bisphenol A, as well as a wide array of micropollutants due to the use of industrial chemicals, biocides, and pharmaceuticals and personal care products.[8]

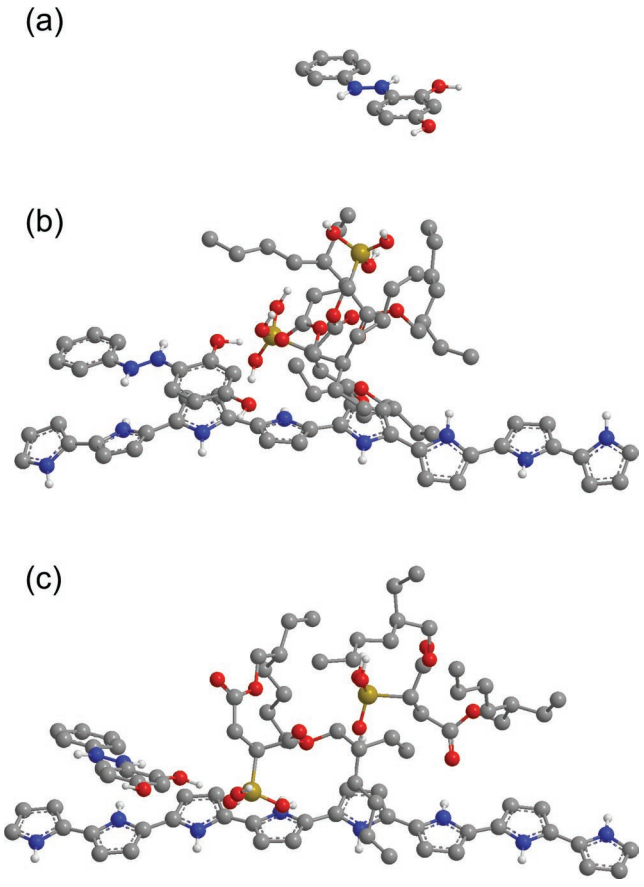


**Figure 4.** Optimized geometries of part (a) a Sudan Orange G molecule interacting with part (b) reduced, and c) oxidized PPy(AOT) complexes.

### 2.3. Highly Porous Morphology

Besides the ability to respond to the electrochemical redox stimuli and modulate affinity for contaminant molecules, the P-PPy(AOT)-based adsorbent also has a key feature—a highly porous morphology—which manifests a threefold improvement over the NP-PPy(AOT): surface roughness for leading to superhydrophobicity in oxidized P-PPy(AOT),[18,23–26] high surface area for adsorbing pollutant molecules as evidenced by higher $K_d$ values described above, and porous structure for exposure to electrolyte solution during the electrochemical redox reaction,[34] as discussed below.

#### 2.3.1. Enhanced Electrochemical Responses

The porosity of P-PPy(AOT) significantly enhances the electrochemical performance of the electrode by increasing the exposure of the polymer to the electrolyte solution during electrochemical redox reactions.[34] Both types of PPy(AOT) demonstrated a pair of redox peaks: the anodic and cathodic peaks observed in their cyclic voltammetry (CV) profiles are around

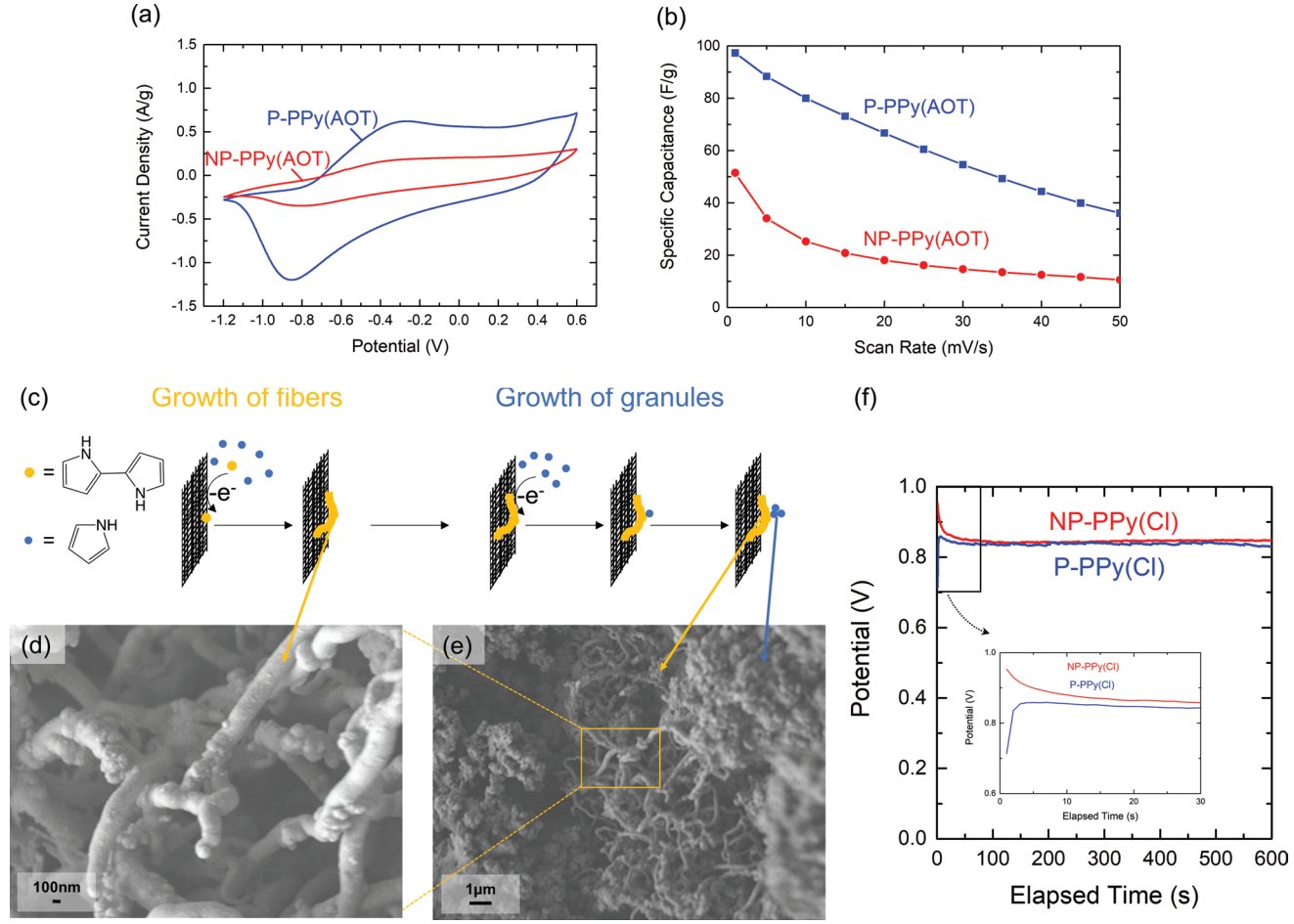


**Figure 5.** a) CV profiles of P-PPy(AOT) at various scan rates (blue) and NP-PPy(AOT) (red) (supporting electrolyte 0.1 M NaCl). b) The specific capacitance of P-PPy(AOT) (blue) and NP-PPy(AOT) (red) as a function of CV scan rates. c) A schematic illustration for the proposed mechanism of forming a highly porous morphology in the PPy film due to the temporally segregated growth of the fibrillar and the granular structures. HRSEM images of (d) PPy(Cl) fibers forming an underlying network on top of which (e) granular structures are deposited. f) Chronopotentiometric potential–time curves of the electropolymerization process of P- and NP-PPy(Cl) in the presence (blue) or absence of bipyrrole (red), respectively.

–0.8 and –0.4 V (versus Ag/AgCl), characteristic of insertion and expulsion of sodium ($Na^+$) ions, respectively (**Figure 5**a).[17] However, NP-PPy(AOT) exhibited a pair of less prominent redox peaks, a larger peak separation, and smaller current density, suggesting that the $Na^+$ reaction kinetics was slower, likely due to reduced surface accessibility.[35] The specific capacitance of the P- and NP-PPy(AOT) was calculated from the CV curves at various scan rates according to the equation:

$$C = \frac{\int I\,dV}{vmV} \tag{4}$$

where $C$ is the specific capacitance (F $g^{-1}$) based on the mass of polymer, $I$ is the current (A), $V$ is the potential (V), and $v$ is the potential scan rate (V $s^{-1}$). Figure 5b reveals that the specific capacitance of P-PPy(AOT) is more than double that of NP-PPy(AOT) at various scan rates ranging from 1 to 50 mV $s^{-1}$. The superior electrochemical performance of P-PPy(AOT), as evidenced by the shape of the CV curve and higher specific capacitance, can be attributed to the larger surface area afforded by the microstructures in P-PPy(AOT) for interaction with the electrolyte. The CV profiles also suggested that potentials of +0.5 and –0.8 V (versus Ag/AgCl) be applied for driving complete oxidation and reduction of PPy(AOT) films, respectively. We analyzed the high-resolution N1s core-level XPS spectra of oxidized and reduced P-PPy(AOT), which were deconvoluted into four peaks to confirm the redox actuations—the reduced P-PPy(AOT) contains higher portions of neutral nitrogen atoms than does the oxidized polymer (Figure S2c,d, Supporting Information).

### 2.3.2. Formation of the Porous Morphology

The highly porous structures offer many benefits to P-PPy(AOT) as an electrochemically regenerable adsorbent. It is therefore of interest to understand mechanistically the formation of the morphology. Previous studies have reported that the amphiphilic nature of AOT can influence the morphology of PPy by aligning the monomers during chemical oxidative polymerization.[36,37] In order to investigate the impact of bipyrrole alone on the morphology of the electropolymerized

PPy and exclude any confounding factors associated with AOT, we used sodium chloride (NaCl) solution as the electrolyte to provide chloride ions (Cl) for doping the polymer. A similar phenomenon was observed: the addition of bipyrrole induced hierarchical porous structures in the PPy(Cl) film (Figure S1a,b, Supporting Information), suggesting that the formation of the unique morphology in the PPy film, independent of the doping anions, was due to the presence of bipyrrole in the electropolymerization bath.

Figure 5c illustrates schematically our hypothesis for the morphological evolution of electropolymerized PPy in the presence of bipyrrole which induced temporally segregated growth of the fibrillar and the granular structures. The two types of microstructures combined to form a highly porous interconnecting network of PPy aggregates. The electropolymerization of pyrrole begins with the oxidation of monomers to form radical cations which then react with other monomers present in the solution to form dimers, oligomers and eventually polymers.[38] The extended conjugation in the PPy oligomers or polymers lowers the oxidation potential compared to that of the monomer.[38] As a result, the slow dimerization of pyrrole is the rate-limiting step.[39] This explains the shape of the potential–time curves of the galvanostatic electropolymerization process of NP-PPy(Cl) formed in the absence of bipyrrole—the potential decreased at early times and eventually leveled off (Figure 5f).

The introduction of pyrrole dimers to the electropolymerization bath accelerated the rate of polymerization by allowing chain extension to occur from the added bipyrrole nuclei before pyrrole monomers completed the slow dimerization step on the electrode surface. Sufficiently fast polymerization favors homogeneous nucleation and generates nanofibrillar structures,[39] which are observed to be embedded in granular PPy(Cl) networks in the high-resolution scanning electron microscopy (HRSEM) image (Figure 5d). As these oligomeric nanofiber chains surpassed the solubility limit, they precipitated onto the electrode surface. At later times, dimerization of pyrrole monomers occurred on the electrode surface or along the PPy nanofibers previously formed. Due to the retardation of dimerization and high concentration of pyrrole monomers, heterogeneous nucleation was dominant at later stages and resulted in the growth of granular PPy particles on the PPy nanofibrillar structures, as seen in Figure 5e. Figure 5f shows that the shape of the potential–time curve for P-PPy(Cl) electropolymerization was different from that of NP-PPy(Cl), further corroborating our hypothesis. The initial increase in potential indicates that chain extension from bipyrrole readily takes place at the outset of electropolymerization, while the dimerization of pyrrole monomer slowly catches up at a higher potential with 10 s delay (Figure 5f inset). The accumulation of pyrrole oligomers gradually led to a decrease in the oxidation potential required for further chain extension and eventually reached a constant level, similar to the case of NP-PPy(Cl). The potential–time curves had similarly distinct shapes that depended on the presence of bipyrrole when the electrolyte used was NaAOT instead of NaCl during electropolymerization (Figure S2e,f, Supporting Information). Therefore, the highly porous morphology of PPy(AOT) formed in the presence of bipyrrole was induced by a mechanism similar to that proposed above, irrespective of the doping anions used.

### 2.4. Electrochemically Reversible Adsorption

The high capacity for neutral organic molecules, as well as the electrochemically controlled affinity, suggest that P-PPy(AOT) is an effective adsorbent material for removing neutral organic pollutants from water with potential for repeated use in cyclic operations. Desorption of dye molecules from traditional adsorbents has remained a challenge, especially without the aid of heat, pH adjustment or organic solvent.[40] In our case, however, the distinct affinities of oxidized and reduced P-PPy(AOT) for organic contaminants can be exploited to regenerate the adsorbent. To demonstrate the recyclability of P-PPy(AOT) for removing neutral organic molecules from water in the micromolar range, we conducted five consecutive cycles of sorption experiments with $0.01 \times 10^{-3}$ M or 2.14 mg $L^{-1}$ SOG aqueous solutions. As illustrated in **Figure 6**a, each sorption cycle began with a P-PPy(AOT)-coated carbon cloth electrode in the oxidized state (+0.5 V versus Ag/AgCl). After adsorption of SOG reached equilibrium, the electrode potential was reduced to –0.8 V (versus Ag/AgCl) in an aqueous stripping solution containing NaCl as the supporting electrolyte. Subsequently, the electrode was re-oxidized in the same NaCl solution used in the reduction step to reactivate the P-PPy(AOT). This re-oxidation step marked the completion of one sorption cycle and regenerated the electrode for another cycle of adsorption. During the five cycles, we observed limited decay in adsorption capacity (Figure 6b), which demonstrated the reusability of P-PPy(AOT).

The nearly complete restoration of adsorption capacity in P-PPy(AOT) exhausted by electrochemical reduction suggested that all of the SOG molecules adsorbed in the previous cycle should have been released to free up sites for SOG uptake in the subsequent cycle. Interestingly, during the electrochemical reduction of P-PPy(AOT), we observed that shortly after the onset of electrochemical reduction, SOG adsorbed on the electrode started to be released from the solid to the stripping solution, as indicated by the yellow color of the solution (Figure 6c, and Movie S5, Supporting Information). However, after a contact period of several minutes, the stripping solution began to clarify instead of becoming darker, while the reduction potential was still being applied. This could be due to the electrochemical reduction of the azo compound SOG released during the regeneration.[41]

Figure 6d shows the potential electrochemical reduction pathway of SOG in aqueous media: a two-electron reduction leads to hydrogenation of the azo group to hydrazo, and the N–N bond can be cleaved by a further two-electron reduction reaction. The hydrazo product of SOG reduction (II) was detected in the aqueous stripping solution after regeneration of P-PPy(AOT) by electrochemical reduction using liquid chromatography–mass spectrometry (Figure S6b,c, Supporting Information). Because the pH of the stripping solution was neutral, only the first reduction reaction took place, and further reduction of the hydrazo compound leading to the N–N bond cleavage was not observed. Such electrochemical reduction of SOG to its hydrazo counterpart can be reversed as the azo-hydrazo redox reaction is reversible in protic media, allowing SOG to be recycled if desired.[41] The relative amounts of SOG and the hydrazo compound in the final stripping solution will depend on the rate of desorption relative to the kinetics of the

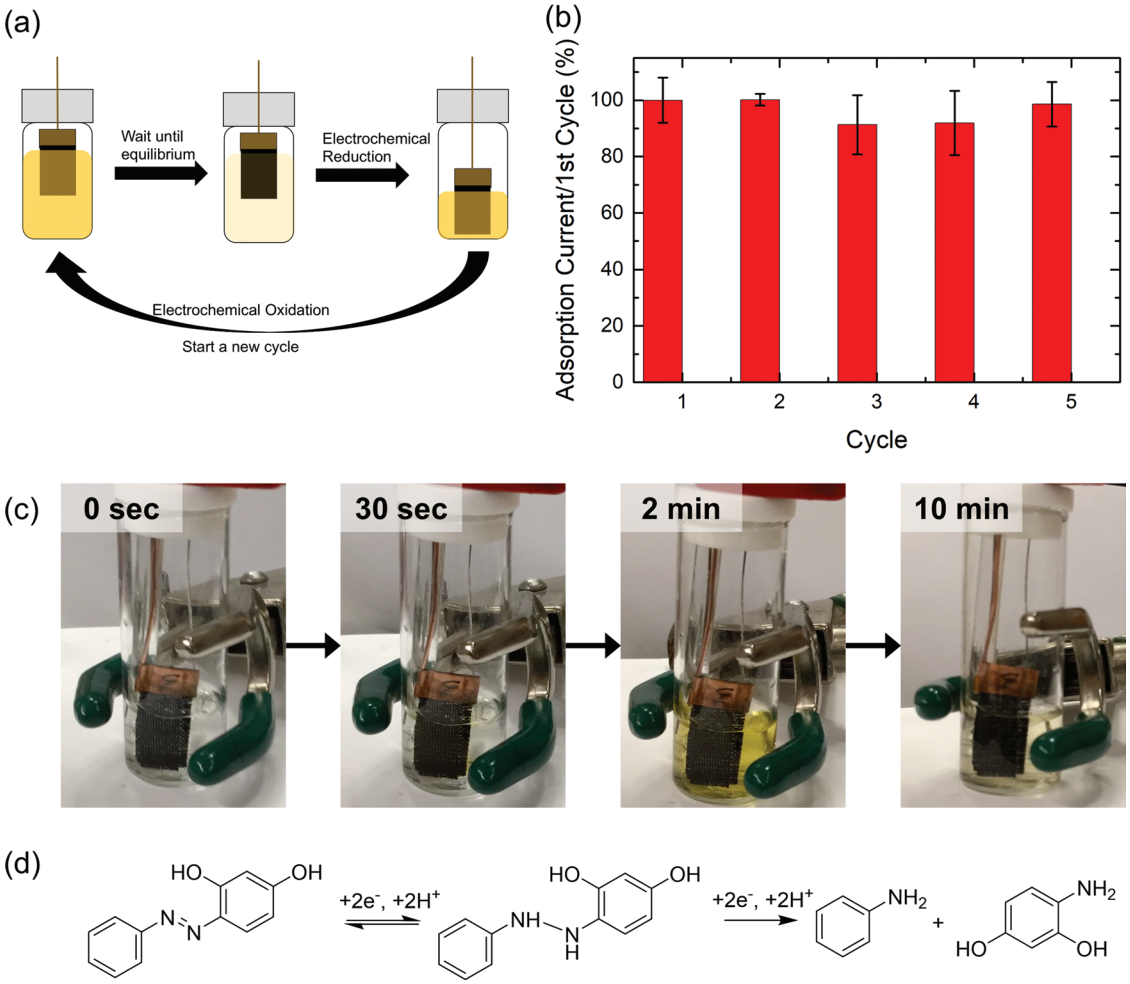


**Figure 6.** a) A schematic of the electrochemically reversible adsorption process of the P-PPy(AOT) coated on a carbon fiber cloth electrode. b) Over five cycles, the adsorption capacity of P-PPy(AOT) remained above 90% of the capacity of the first cycle. c) Snapshots of the desorption video (Movie S5, Supporting Information). To accentuate the color change, the video was taken with an electrode equilibrated with a more concentrated SOG solution. Section S5 and Movie S6 in the Supporting Information presents the desorption step during the cyclic sorption of $0.01 \times 10^{-3}$ M SOG solutions where the color change was less dramatic. d) A potential pathway for the electrochemical reduction of SOG.[41]

reduction reaction. If reaction kinetics is slower than release rates, then the released product can be removed intact by minimization of the contact time during desorption.

The electrochemical reduction of P-PPy(AOT) renders the polymer more hydrophilic, due to the re-arrangement of AOT relative to the polymer backbone, to induce the desorption of the adsorbed SOG molecules. This desorption, in combination with an electrochemically catalyzed reduction of SOG, regenerates the functional material to regain full capacity for adsorption of SOG in subsequent cycles.

We carried out 100 repeated reduction and oxidation cycles to test the stability of the P-PPy(AOT) adsorbent by tracking the atomic compositions of the film using XPS. The polymer and its dopants are intact up to 50 cycles with almost no change in the compositions, while some degradation or dissolution of the polymer film is observed at the 75th and 100th cycles. Nevertheless, the nearly complete restoration of the adsorption capacity of P-PPy(AOT) over five cycles and the ability to retain AOT in the polymer film after extended cycles demonstrate the robustness of P-PPy(AOT) for reversible sorption of neutral organic pollutants from water (Table S4, Supporting Information).

## 3. Conclusion

In conclusion, we have developed a facile method to synthesize highly porous homogeneous CPs on carbon fiber cloths by electrochemical polymerization of pyrrole with a trace amount of bipyrrole and simultaneous doping of the polymer with surfactant anions. The resulting P-PPy(AOT) is superhydrophobic in the oxidized state and exhibits electrochemically tunable hydrophobicity. Our MD-DFT simulations corroborate the hypothesis that reorientation of AOT dopants with respect to the polymer backbone during redox processes modulates the hydrophobicity of the polymer. The electrochemically modulated reorientation of the surfactant relative to PPy also facilitates the hydrogen bond formation between the adsorbate and the AOT dopant when PPy is oxidized, increasing the affinity

of the material towards organic molecules. The compositional and morphological advantages lead to the high adsorption capacity and reversibility of P-PPy(AOT) for removing organic micropollutants from water. The understanding of the interactions between dopants, polymer, and adsorbate on the molecular level is significant for developing broader applications of the materials with electrochemically tunable hydrophobicity in drug delivery, sensing, self-cleaning surfaces, microfluidics, and artificial muscles.[15,18,21,42]

## 4. Experimental Section

*Electrode Fabrication and Electrochemical Characterizations*: All electropolymerization and electrochemical characterizations were performed on a VersaSTAT4 potentiostat (Princeton Applied Research) in a three-electrode configuration where the counter electrode was a platinum wire and the reference electrode was Ag/AgCl (BASi). Electropolymerization was carried out by applying a constant current density of 5 mA $cm^{-2}$ for 10 min to a carbon fiber cloth substrate. In a typical preparation of the porous PPy film, the solution for electropolymerization consisted of 5 mL of aqueous solution containing 0.1 M of the corresponding electrolyte, 0.3 M pyrrole, and 0.3 mg $mL^{-1}$ bipyrrole.

*Polymer Characterizations*: SEM images were taken using JEOL-6010LA and JEOL-6700 SEMs for regular and high-resolution imaging, respectively. AFM was performed on Veeco Nanoscope V with Dimension 3100 in tapping mode and the images were analyzed using the Nanoscope Analysis software. The contact angles formed by a 2 µL water droplet on a polymer-coated stainless-steel substrate were measured using a Ramé–Hart goniometer at room temperature. Computational details about the DFT–MD simulations can be found in the Supporting Information.

## Supporting Information

Supporting Information is available from the Wiley Online Library or from the author.

## Acknowledgements

This research was supported by a grant from the J-WAFS Annual Seed Grant Program. The DFT calculations and MD simulations were supported by a grant from the U.S. Department of Energy, Basic Energy Sciences (BES ER46474). This work made use of the Cornell Center for Materials Research Shared Facilities which are supported through the NSF MRSEC program (DMR-1719875). The authors would like to thank Yiming Mo for the helpful discussion on the electrochemical reduction of azo compounds.

## Conflict of Interest

The authors declare no conflict of interest.

## Keywords

electrochemical regeneration, hydrophobicity, polypyrrole, separations, surfactant

Received: February 26, 2018
Revised: May 4, 2018
Published online: June 22, 2018

[1] "USGS Fact Sheet FS-027-02, Pharmaceuticals, Hormones, and Other Organic Wastewater Contaminants in U.S. Streams," can be found under, https://toxics.usgs.gov/pubs/FS-027-02/ (accessed: June 2018).
[2] L. Lamastra, M. Balderacchi, M. Trevisan, *MethodsX* **2016**, *3*, 459.
[3] R. P. Schwarzenbach, B. I. Escher, K. Fenner, T. B. Hofstetter, C. A. Johnson, U. von Gunten, B. Wehrli, *Science* **2006**, *313*, 1072.
[4] S. D. Richardson, T. A. Ternes, *Anal. Chem.* **2014**, *86*, 2813.
[5] K. E. Murray, S. M. Thomas, A. A. Bodour, *Environ. Pollut.* **2010**, *158*, 3462.
[6] N. W. Brown, E. P. L. Roberts, A. A. Garforth, R. A. W. Dryfe, *Electrochim. Acta* **2004**, *49*, 3269.
[7] A. Sayari, S. Hamoudi, Y. Yang, *Chem. Mater.* **2005**, *17*, 212.
[8] A. Alsbaiee, B. J. Smith, L. Xiao, Y. Ling, D. E. Helbling, W. R. Dichtel, *Nature* **2016**, *529*, 190.
[9] B. Karabacakoğlu, Ö. Savlak, *Ind. Eng. Chem. Res.* **2014**, *53*, 13171.
[10] H. Kusic, N. Koprivanac, A. L. Bozic, *Chem. Eng. J.* **2006**, *123*, 127.
[11] A. Akhoury, L. Bromberg, T. A. Hatton, *ACS Appl. Mater. Interfaces* **2011**, *3*, 1167.
[12] X. Mao, W. Tian, J. Wu, G. C. Rutledge, T. A. Hatton, *J. Am. Chem. Soc.* **2015**, *137*, 1348.
[13] X. Mao, W. Tian, Y. Ren, D. Chen, S. E. Curtis, M. T. Buss, G. C. Rutledge, T. A. Hatton, submitted.
[14] D. Mecerreyes, V. Alvaro, I. Cantero, M. Bengoetxea, P. a. Calvo, H. Grande, J. Rodriguez, J. a. Pomposo, *Adv. Mater.* **2002**, *14*, 749.
[15] J. Isaksson, C. Tengstedt, M. Fahlman, N. Robinson, M. Berggren, *Adv. Mater.* **2004**, *16*, 316.
[16] Y.-J. Qiu, J. R. Reynolds, *Polym. Eng. Sci.* **1991**, *31*, 417.
[17] K. P. Vidanapathirana, M. A. Careem, S. Skaarup, K. West, *Solid State Ion.* **2002**, *154–155*, 331.
[18] L. Xu, W. Chen, A. Mulchandani, Y. Yan, *Angew. Chem. Int. Ed.* **2005**, *44*, 6009.
[19] J. An, J.-F. Cui, Z.-Q. Zhu, W.-D. Liang, C.-J. Pei, H.-X. Sun, B.-P. Yang, A. Li, *J. Appl. Polym. Sci.* **2014**, *131*, 9197.
[20] O. US EPA, "Drinking Water Health Advisories for PFOA and PFOS," can be found under, https://www.epa.gov/ground-water-and-drinking-water/drinking-water-health-advisoriesp-foa-and-pfos, (accessed: June 2018).
[21] Y.-T. Tsai, C.-H. Choi, N. Gao, E.-H. Yang, *Langmuir* **2011**, *27*, 4249.
[22] L. Li, Y. Bai, L. Li, S. Wang, T. Zhang, *Adv. Mater.* **2017**, *29*, 1702517.
[23] D. Ge, S. Huang, R. Qi, J. Mu, Y. Shen, W. Shi, *Chem. Phys. Chem* **2009**, *10*, 1916.
[24] N. A. Patankar, *Langmuir* **2004**, *20*, 8209.
[25] A. Lafuma, D. Quéré, *Nat. Mater.* **2003**, *2*, 457.
[26] J. H. Chang, I. W. Hunter, *Macromol. Rapid Commun.* **2011**, *32*, 718.
[27] A. Kuleyin, *J. Hazard. Mater.* **2007**, *144*, 307.
[28] P. R. Horn, M. Head-Gordon, *J. Chem. Phys.* **2016**, *144*, 084118.
[29] P. S. Bagus, C. J. Nelin, D. A. Hrovat, E. S. Ilton, *J. Chem. Phys.* **2017**, *146*, 134706.
[30] P. R. Horn, Y. Mao, M. Head-Gordon, *Phys. Chem. Chem. Phys.* **2016**, *18*, 23067.
[31] W. Pauli, *Z. Für Phys.* **1925**, *31*, 765.
[32] T. Steiner, *Angew. Chem. Int. Ed.* **2002**, *41*, 48.
[33] X. Su, H. J. Kulik, T. F. Jamison, T. A. Hatton, *Adv. Funct. Mater.* **2016**, *26*, 3394.
[34] W. Tian, X. Mao, P. Brown, G. C. Rutledge, T. A. Hatton, *Adv. Funct. Mater.* **2015**, *25*, 4803.
[35] K. L. Hawthorne, J. S. Wainright, R. F. Savinell, *J. Electrochem. Soc.* **2014**, *161*, A1662.
[36] J. Jang, H. Yoon, *Langmuir* **2005**, *21*, 11484.

 

[37] K. Boukerma, M. Omastová, P. Fedorko, M. M. Chehimi, *Appl. Surf. Sci.* **2005**, *249*, 303.
[38] S. Sadki, P. Schottland, N. Brodie, G. Sabouraud, *Chem. Soc. Rev.* **2000**, *29*, 283.
[39] H. D. Tran, Y. Wang, J. M. D'Arcy, R. B. Kaner, *ACS Nano* **2008**, *2*, 1841.
[40] X. Zhuang, Y. Wan, C. Feng, Y. Shen, D. Zhao, *Chem. Mater.* **2009**, *21*, 706.
[41] J. Jaworski, in *Org. Electrochem*. 5th Ed., CRC Press, **2015**, p. 1121.
[42] S. Skaarup, L. Bay, K. Vidanapathirana, S. Thybo, P. Tofte, K. West, *Solid State Ion.* **2003**, *159*, 143.